# Mechanical properties and deformation-driven band gap tuning on [N]-Carbophenes

Gabriel H. Batista<sup>a</sup>, Chad E. Junkermeier<sup>b</sup>, George Psofogiannakis<sup>c</sup>, Ricardo Paupitz<sup>a,1,\*</sup>

<sup>a</sup> Physics Department, IGCE, São Paulo State University, UNESP, 13506-900, Rio Claro, SP, Brazil
 <sup>b</sup> Materials Computation Laboratory, University of Hawai'i Maui College, Kahului HI 96732, USA
 <sup>c</sup> Department of Chemical and Biological Engineering, University of Ottawa, Canada

#### **Abstract**

A new class of two-dimensional carbon-based materials, N-carbophenes, is studied using tight binding density functional theory. The present study addresses the influence of strain on band gap opening for N-Carbophenes where  $3 \le N \le 9$ . We found that both uniaxial and biaxial strains can lead to significant changes in the electronic structure of N-carbophenes. One unexpected effect was the existence of a maximum value for the band gaps for strains in the range  $13\% \le \varepsilon \le 15\%$  and that increasing  $\varepsilon$  above that range can cause a reduction in the band gap. The origin of the band gap openings is due to the stretching of C-C bonds in the N-carbophene 4-member rings.

Keywords: phenylene, carbophene, graphenylene, covalent organic framework, porous materials, 2-dimensional materials

#### 1. Introduction

Two-dimensional (2D) materials have attracted a lot of attention for their fascinating and attractive properties. The possibility of using these materials in devices such as diodes, transistors [1, 2], sensors [3], batteries [4, 5], etc., triggered many studies of their properties. Part of the motivation for investigating many new 2D materials in the last decade was that it was impossible to completely overcome the practical difficulties imposed by graphene's semi-metallic nature. One option to overcome the obstacles related to graphene's closed band gap would be to adjust it by some external action. Previous studies reported harnessing this possibility in several ways, such as cutting the material into nanoribbons (GNRs) [6], introducing defects [7], functionalization [8, 9], and applying strain [10]. Another option that has been studied is the use of two-dimensional materials, such as graphenylene, porous graphene [11], hexagonal boron nitride, porous boron nitride, and inorganic graphenylene

In 2017, Du *et al.* reported that they may have synthesized a new 2D carbon-based material, 3-carbophene [13]. The structure of 3-carbophene is based on arrangements of linear phenylenes, resulting in a porous hexagonal geometry, see Figure 1. Junkermeier and collaborators expanded the idea of 3-carbophene into a class of materials, the N-carbophenes. They demonstrated that pristine N-carbophenes are energetically favorable to the similarly structured graphenylene and are semiconductors with band gaps between 1.2 eV and 1.9 eV[14]. They further demonstrated that replacing the H atoms with functional groups lowers the formation energies and changes

the band gaps depending on the type of functional group and the degree of functionalization[15].

To contribute to the search for new materials, we explore the electromechanical properties of N-carbophenes. This work investigates applying uniaxial and biaxial strain on pristine N-carbophene structures to control their electronic properties. Using tight-binding density functional theory (DFTB), we studied many configurations and demonstrated that N-carbophenes' band gaps could be increased or decreased significantly depending on the value and type of strain applied. Simulations of stretched linear 3-phenylene are used to clarify the origins of band gap variations in N-carbophenes.

## 2. Methodology

Before carrying out the tests necessary to calculate the mechanical and electronic properties, geometry optimizations were performed using the DFTB approximation implemented in the DFTB+ software [16, 17, 18, 19]. DFTB+ has accuracy comparable to density functional theory (DFT) when applied to electronic structure calculations while being significantly faster than most DFT codes. Much of this speed-up comes from the use of look-up tables (located in the so-called Slater-Koster files) instead of performing integral evaluations at runtime. In our simulations, we used the *matsci Slater-Koster files*, which were constructed to describe materials' science problems [20, 21].

For geometry optimization, including the cell parameters and atomic positions within the cell, a conjugate gradient algorithm was used, imposing a maximum force difference of  $10^{-3}$  eV/Å and a maximum tolerance of  $10^{-4}$  eV on energy variation as convergence criteria. Numerical convergence tests were used to determine the number of k-points needed in Monkhorst-Pack grids. A 16x16x1 Monkhorst-Pack k-point grid was used for

<sup>\*</sup>Email: ricardo.paupitz@unesp.br

<sup>&</sup>lt;sup>1</sup>Present address: Université Claude Bernard - Lyon 1, CNRS, Institut Lumière Matière, F-69622 Lyon, France

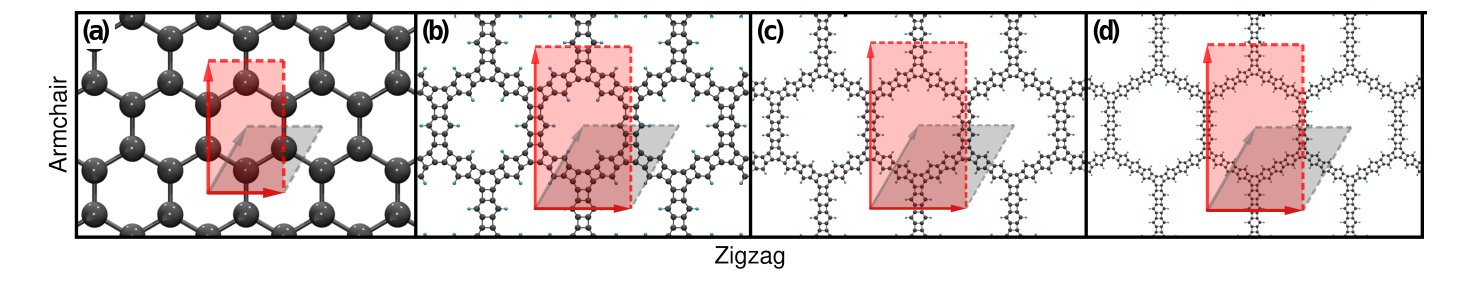


Figure 1: Representative examples of structural models considered in this work. (a) Graphene, with two atoms in the unit cell, (b) 3-carbophene, with 36 atoms in the unit cell, (c) 4-carbophene, with 60 atoms in the unit cell, and (d) 5-carbophene, with 84 atoms in the unit cell. The unit cell is highlighted in light gray in each case. In light red, the rectangular supercells used during the simulations of this work are highlighted, containing twice as many atoms as the unit cell. Additionally, armchair and zigzag directions are defined.

cell optimization, while during the density of state (DOS) calculations, a 48x48x1 Monkhorst-Pack k-point grid was used. To avoid interactions between the carbophene sheet and its virtual images, a large out-of-plane bounding box size of 30 Å was considered.

To facilitate the application of strain in the structures proposed in the present work, rectangular supercells were used during the simulations; as depicted in Figure 1. To calculate the Young's modulus (Y) and Poisson's ratio  $(\nu)$ , we monitor the change in elastic energy per unit area of the structure (U) during the application of  $\operatorname{strain}(\epsilon)$  in specific directions and fit the results to the expression,

$$U(\epsilon) = \frac{1}{2}C_{11}\epsilon_{arm}^2 + \frac{1}{2}C_{22}\epsilon_{zig}^2 + C_{12}\epsilon_{arm}\epsilon_{zig},\tag{1}$$

where  $\epsilon_{arm}$  and  $\epsilon_{zig}$  are the deformations in the armchair and zigzag directions and  $C_{11}$ ,  $C_{22}$  and  $C_{12}$  are the elastic constants, corresponding to second partial derivatives of the energy with respect to strain. The elastic constants can be obtained by fitting the energy per unit area versus strain curves for each kind of strain (i.e., uniaxial or biaxial). These curves are shown in the Supplementary Materials, Fig. S1 and S2. Thus, we were able to obtain each of the above constants and then calculate Y and  $\nu$  in each direction [22]:

$$Y_{arm} = \frac{\left(C_{11}C_{22} - C_{12}^2\right)}{C_{22}}, \quad Y_{zig} = \frac{\left(C_{11}C_{22} - C_{12}^2\right)}{C_{11}}, \quad (2)$$

$$v_{arm} = \frac{C_{12}}{C_{22}}, \quad v_{zig} = \frac{C_{12}}{C_{11}}.$$
 (3)

To calculate the band gaps, the difference between the conduction band's minimum energy and the valence band's maximum was computed. Because we use rectangular supercells, the high symmetry points  $\Gamma$ , X, S, and Y in the first Brillouin zone of an orthorhombic lattice were used, as described in [23].

#### 3. Results and Discussion

In Table 1, we can see the results for Young's modulus and Poisson's ratio in the *zigzag* and *armchair* directions for 3- to 10-carbophene as defined in Fig. 1, together with the results for graphene, for comparison.

Table 1: Young's moduli (Y) in units of GPa and Poisson's ratios ( $\nu$ ), using DFTB calculations.

System	$Y_{arm}$	$\mathbf{Y}_{zig}$	$\nu_{arm}$	$\nu_{zig}$
graphene	1144.33	1123.92	0.26	0.25
3-carbophene	153.362	153.612	0.592	0.593
4-carbophene	58.122	58.191	0.745	0.746
5-carbophene	29.726	29.248	0.828	0.815
6-carbophene	17.769	17.599	0.867	0.859
7-carbophene	12.479	12.407	0.885	0.880
8-carbophene	8.973	8.905	0.904	0.897
9-carbophene	6.410	6.445	0.915	0.920
10-carbophene	5.421	5.443	0.919	0.923

Comparing our results for graphene with those in the literature, Young's modulus is within the range of values calculated via DFT and DFTB by Memarian (1023.95 - 1395.08 *GPa*) [24] and close to that found experimentally by Lee (1000 *GPa*) [25]. Furthermore, our calculated Poisson's ratio for graphene also approximates values calculated by other authors via molecular dynamics (MD) and DFT (0.16 - 0.22) [26, 27, 28]. Therefore, our results are within those expected for graphene and can give a reasonable description for other carbon-based 2D materials such as N-carbophenes.

In Fig. 1 one can see that, as the N index of carbophenes grows, the system presents larger pores, and consequently lower densities  $\rho$ . For porous materials, Young's modulus has been found to be proportional to some power of the density,  $Y \sim \rho^n$ , where n varies depending on the structure and density of the pores [29]. The scaling variation has been discussed by several authors considering the influence of pore density and geometrical structure on the deformation process [22, 30] and, in some cases, taking into account the change in dimensionality of the material depending on the porosity[31]. For example, the value of n is  $\sim 0.6$  in the case of cubic structures,  $\sim 2.0$  for graphene, and going up to ~3.6 for fractals[32, 29]. In the case of Ncarbophenes, in Fig. 2 we plotted the Young modulus  $Y_{arm}$  and  $Y_{zig}$  against the relative density of each material, taking as reference the density of graphene on a log-log scale. Fitting the data with expressions  $Y_{arm} \sim \rho^{n_{arm}}$  and  $Y_{zig} \sim \rho^{n_{zig}}$  we obtain  $n_{arm} \sim 2.99$  and  $n_{zig} \sim 2.96$  for the higher density structures, and a variation on this scale for the lower density examples, indicating that carbophenes stiffness is significantly more sensitive than graphene to density variations.

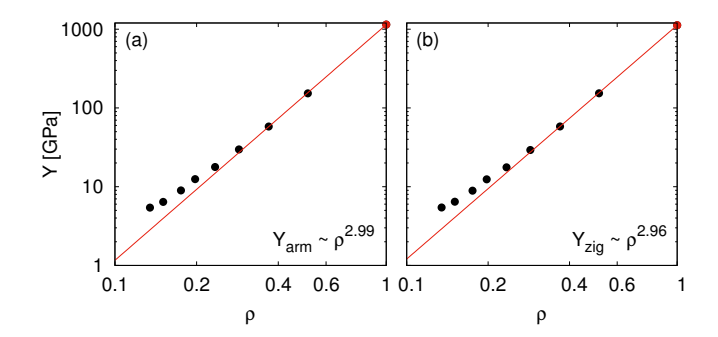


Figure 2: Young moduli calculated along a) armchair direction and (b) zigzag direction versus relative density for N-carbophenes (black circles) and graphene (red circle). The red lines are fits used to obtain the exponents  $n_{arm} = 2.99$  and  $n_{zig} = 2.96$ .

For comparison, we also calculated the mechanical properties of N-carbophenes using Adaptive Intermolecular Reactive Empirical Bond Order (AIREBO) Potential-based MD simulations [33]. The use of this approach allowed the simulation of larger N-carbophene supercells. The details of AIREBO MD simulations and comparison of its results with the DFTB+ results are in Section 2 of Supplementary Materials.

Fig. S5 of the Supplementary Materials shows the band dispersions and DOS of pristine N-carbophenes. The band gap values for N-carbophenes can be seen in Fig. S6. One can see that the results agree with those found in [14], suggesting that the protocols adopted in the present case are consistent with our previous work.

For each material, we performed tensile tests on rectangular supercells, as defined in Figure 1, to monitor the variation of the band gap value under strain. Initially, the size of the armchair side of the relaxed supercell was increased, and then a geometry optimization was performed, maintaining the stretched direction with a fixed length. It is important to note that during the optimization process, the structure does not return to its equilibrium geometry because the lattice vectors are not optimized, causing the periodic boundary condition to hold the structure under a fixed area. Then the band structure was calculated, obtaining the energy values of the frontier orbitals before adding a new strain and proceeding to the next step. Performing this protocol, we generated the data labeled "Uni<sub>arm</sub>" in Figure 3.

The same protocol was applied to the *zigzag* direction (generating "Uni<sub>zig</sub>" in Figure 3) and adapted to the case of biaxial strain, in which the deformation is defined simultaneously for both directions (*armchair* and *zigzag*).

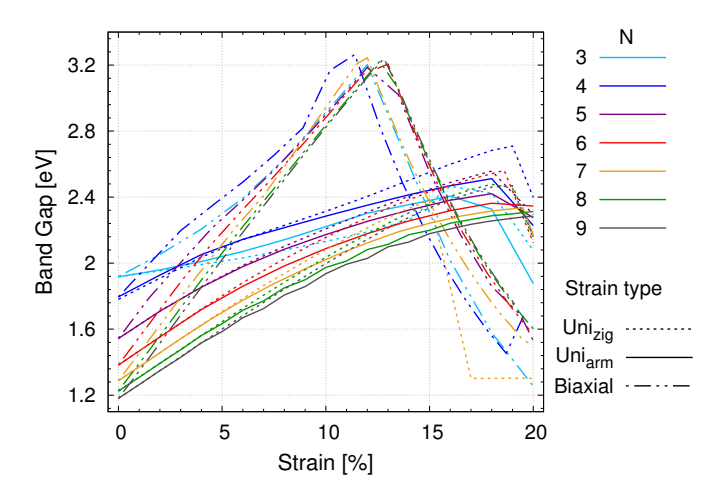


Figure 3: Influence of strain application on gap opening for N-Carbophenes considering  $3 \le N \le 9$ . For biaxial strain, the band gap maxima all occur for strains in a defined range, namely 11%-13%. Uniaxial strain data indicate the presence of a maximum band gap opening for each case, but for much larger deformations, in the range 16%-20%, close to the breaking point for those structures

Our results indicate a similar increase in the band gap values for all N-carbophenes when we apply uniaxial tensile strains. In the armchair and zigzag cases, strains of up to almost 20% resulted in increased band gap values. In the case of biaxial tensile tests, there is an increase in band gap values until approximately 11 to 13 % strain, after which a narrowing of the band gaps is observed as the strain is increased.

N-carbophenes are hexagonal structures in which each "edge" can be interpreted as a linear N-phenylene. To investigate the strain-induced band gap variation of N-carbophenes, we can reduce the problem to just one "edge" of the structure and deform it in one direction. This strategy allowed us to divide the bonds of this edge (N-phenylene) into three types: those that were only part of 6-member rings, those that were only part of the 4-member rings, and those that were shared by both 4- and 6-member rings. Three tests were applied to 3-phenylene (insert Figure 4): First, the entire structure was stretched along the horizontal direction, performing a deformation-optimization process similar to that described above for the N-carbophenes. In this case, in each step the hydrogen atoms bound to the tip atoms were held fixed during the geometry optimization. The second test consisted of deforming bonds that are only part of the 6-member rings (blue bonds in Figure 4 insert) in the strain direction. Lastly, deforming the bonds that are only part of 4-member rings (red bonds in Figure 4 insert) in the strain direction. The differences in highest occupied molecular orbital (HOMO) and lowest unoccupied molecular orbital (LUMO) energy gaps found during those tests are presented in Figure 4. These results demonstrate that the 3phenylene's energy gap is widening due to the stretching of the 4-member ring bonds. Thus, the increase of C-C distances during the deformation diminishes the orbital overlap for neighbor atoms and can increase the amount of energy necessary to promote the hopping of an electron to its nearest neighbor. This causes a decrease in the mobility of charge carriers inside the material, which is related to the marked flatness of the frontier bands after deformation.

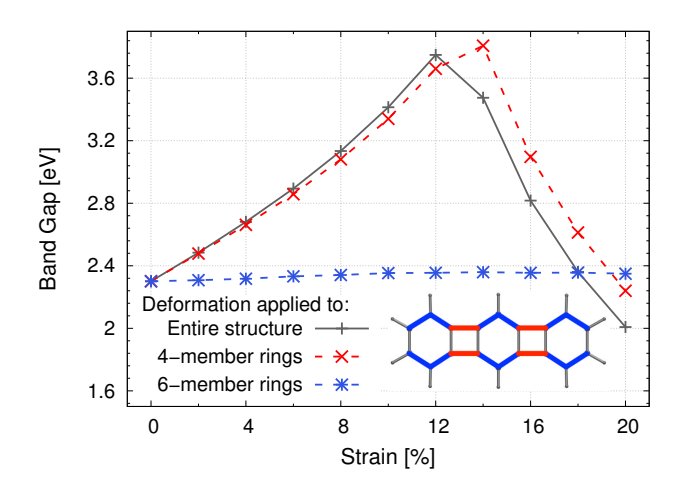


Figure 4: HOMO-LUMO energy gap variation of 3-phenylene when stretched in different ways. Insert: 3-phenylene structure emphasizing the stretched 4-member ring bonds (red) and 6-member ring bonds (blue).

The change in band gap values as a function of strain is a characteristic that draws attention to the data of Figure 3. Looking in detail at the band structures shown in Figure 5, one can see that stretching modifies many bands, and some of them are directed toward lower energy values as the strain increases. As the strain gets larger, these bands occupy lower energy values until one becomes the lowest-energy unoccupied band, consequently decreasing the gap.

Figure 5 shows the band structures obtained during the tensile tests applied to N-carbophenes. In that figure, we highlight in red the band which, after the band gap peak, becomes the lowest energetic above the Fermi level. Its contribution to the projected density of states (PDOS) can be identified as the lowest energy *s* orbitals above the Fermi level, plotted in green in the same figure.

During the tensile tests, the geometry optimizations caused variations in the positions of atoms in each strain step, so the shape of the N-carbophenes structure underwent some changes. By monitoring the deformations, we found two distinct behaviors. First, taking the rectangular 3-carbophene supercell as an example, we separate the atoms that constitute it into two groups depicted as red and green in Figure 6. The red (green) group is composed of two subgroups of carbon atoms located along the zigzag (armchair) direction of the supercell, as can be seen in the inset of Figure 6.

During the application of strain in the zigzag direction, the change in lengths and angles of bonds connecting the red atoms was greater than observed in green atoms. Then, by calculating the Projected Density of States (PDOS) for these two groups, it was possible to clarify the contribution of each group of atoms to the frontier orbitals during the strain application. For example, the PDOS and the band structure of 3-carbophene with a zigzag strain of 20%, in Figure 6, demonstrate that the band that becomes the conduction band for high strain values in the zigzag direction, as described earlier, is formed entirely by the

combination of orbitals from atoms of the red group. While for the 20% strain in the armchair direction, the LUMO is composed of the red group atoms.

When strain is applied in the armchair direction, the green atoms positions are more intensely affected than the red atoms. Thus, the upper right graph of the same figure shows that 20% strain in the armchair direction results in a different configuration of PDOS peaks. In this case, the group marked in red has a smaller contribution to the PDOS.

A biaxial strain applied to the material deforms both groups similarly. As expected, there are relevant contributions from both in LUCO, as we can see in the representation of PDOS in the lower right graph still in Figure 6.

#### Conclusion

This work analyzed the band gaps of strained N-carbophenes, where  $3 \le N \le 10$ . The Young's modulus decreased as N increased, going from  $\sim 153 GPa$  for N= 3 up to  $\sim 5.4 GPa$  for N= 10 in both the armchair and zigzag directions. At the same time, the Poisson ratio increased from  $\sim 0.59$  up to  $\sim 0.9$  for both directions. The electronic effects obtained by applying strain were also considered in our analysis, revealing that the band gap opening can be tuned. Uniaxial strains had a maximum band gap opening above 2 eV for all N-carbophenes considered in this work. While biaxial strain resulted in band gaps of up to 3.2eV for strains in the range 11%-13% with a decrease from this value for strains beyond that range. Using linear 3-phenelyne as a simplified model for N-carbophenes, the origin of the band gap openings was found to result from the stretching of C-C bonds in 4-member rings.

## Acknowledgement

Greenwood: A library for creating molecular models and processing molecular dynamics simulations was used to produce the atomic structure models [34]. C. Junkermeier was supported by the United States National Science Foundation under Award Number 2113011 and the University of Hawai'i Information Technology Services Cyberinfrastructure. In addition, R. Paupitz acknowledges Brazilian funding agencies: FAPESP (grants #2018/03961-5 and #2021/14977-2) and CNPq (grants #437034/2018-6 and #315008/2020-2) and computing resources supplied by the Center for Scientific Computing (NCC/GridUNESP) of the São Paulo State University (UNESP). Also, this work used resources of the Centro Nacional de Processamento de Alto Desempenho em São Paulo (CENAPAD-SP).

### CReDiT authorship contribution statement

Gabriel H. Batista: Carried out the simulations, Investigation, Analysis, Visualization, Writing original draft, Writing review & editing. Ricardo Paupitz: Data curation, Investigation, Resources, Visualization, Writing original draft, Writing review & editing. Chad E. Junkermeier: Conceptualization, Project administration, Software, Writing review & editing.

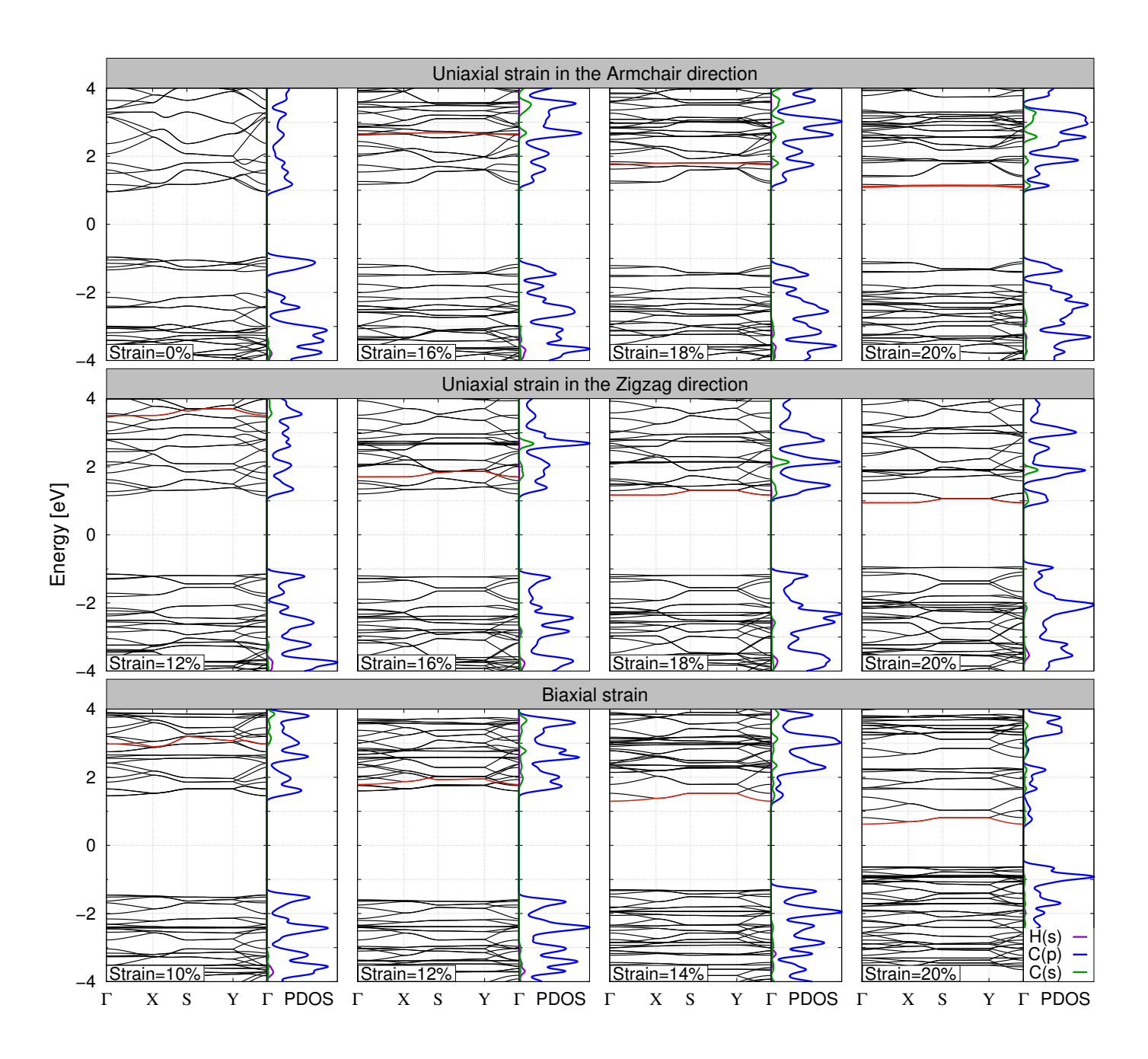


Figure 5: Band structures and projected densities of states (PDOS) of 3-Carbophene were calculated during the three different tensile tests. Curves highlighted in red identify the band which will become the conduction band when the maximum strain is applied. Green curves in the PDOS graph indicate densities related to carbon's *s* orbitals.

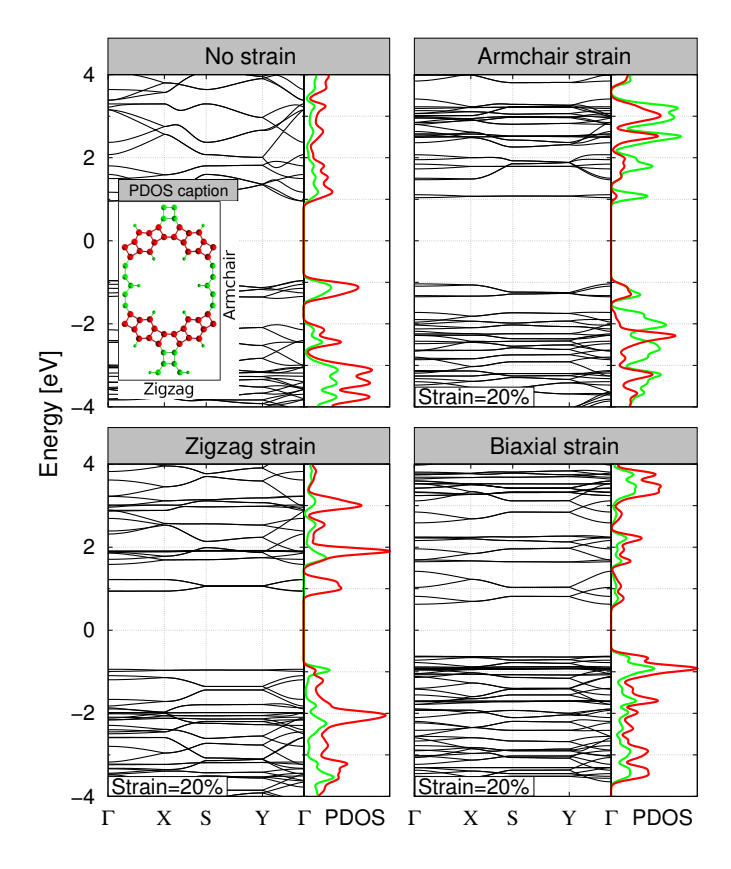


Figure 6: Band structure and PDOS of 3-carbophene in the absence of strain and with strain=20% in the three types of tensile tests performed in this work. Red and green atoms in the inset identify the two different behaviors during tensile tests discussed in the text. Red(green) PDOS curves indicate projection on atoms identified by the same color, namely red(green).

- F. Giannazzo, G. Greco, F. Roccaforte, S. S. Sonde, Vertical transistors based on 2d materials: Status and prospects, CRYSTALS 8 (2). doi:10.3390/cryst8020070.
- [2] S.-K. Su, C.-P. Chuu, M.-Y. Li, C.-C. Cheng, H.-S. P. Wong, L.-J. Li, Layered semiconducting 2d materials for future transistor applications, SMALL STRUCTURES 2 (5). doi:10.1002/sstr.202000103.
- [3] E. W. Hill, A. Vijayaragahvan, K. Novoselov, Graphene sensors, IEEE Sensors Journal 11 (12) (2011) 3161–3170. doi:10.1109/JSEN.2011.2167608.
- [4] L. Peng, Y. Zhu, D. Chen, R. S. Ruoff, G. Yu, Two-dimensional materials for beyond-lithium-ion batteries, ADVANCED ENERGY MATERIALS 6 (11). doi:10.1002/aenm.201600025.
- [5] K.-S. Chen, I. Balla, N. S. Luu, M. C. Hersam, Emerging opportunities for two-dimensional materials in lithium-ion batteries, ACS ENERGY LETTERS 2 (9) (2017) 2026–2034. doi:10.1021/acsenergylett.7b00476.
- [6] V. Barone, O. Hod, G. E. Scuseria, Electronic structure and stability of semiconducting graphene nanoribbons, Nano Letters 6 (12) (2006) 2748–2754, pMID: 17163699. arXiv:https://doi.org/10.1021/nl0617033, doi:10.1021/nl0617033.
  - URL https://doi.org/10.1021/n10617033
- [7] F. Banhart, J. Kotakoski, A. V. Krasheninnikov, Structural defects in graphene, ACS Nano 5 (1) (2011) 26–41, pMID: 21090760. arXiv:https://doi.org/10.1021/nn102598m, doi:10.1021/nn102598m. URL https://doi.org/10.1021/nn102598m
- [8] R. Quhe, J. Ma, Z. Zeng, K. Tang, J. Zheng, Y. Wang, Z. Ni, L. Wang, Z. Gao, J. Shi, J. Lu, Tunable band gap in few-layer graphene by surface adsorption, SCIENTIFIC REPORTS 3. doi:10.1038/srep01794.
- [9] H. Liu, Y. Liu, D. Zhu, Chemical doping of graphene, JOUR-NAL OF MATERIALS CHEMISTRY 21 (10) (2011) 3335–3345. doi:10.1039/c0jm02922j.

- [10] Z. H. Ni, T. Yu, Y. H. Lu, Y. Y. Wang, Y. P. Feng, Z. X. Shen, Uniaxial strain on graphene: Raman spectroscopy study and bandgap opening, ACS Nano 3 (2) (2009) 483–483, pMID: 19583275. arXiv:https://doi.org/10.1021/nn8008323, doi:10.1021/nn8008323. URL https://doi.org/10.1021/nn8008323
- [11] G. Brunetto, P. A. S. Autreto, L. D. Machado, B. I. Santos, R. P. B. dos Santos, D. S. Galvao, Nonzero gap two-dimensional carbon allotrope from porous graphene, Journal of Physical Chemistry C 116 (23) (2012) 12810–12813. doi:10.1021/jp211300n. URL <Go to ISI>://WOS:000305356200053
- [12] E. Perim, R. Paupitz, P. A. S. Autreto, D. S. Galvao, Inorganic graphenylene: A porous two-dimensional material with tunable band gap, JOUR-NAL OF PHYSICAL CHEMISTRY C 118 (41) (2014) 23670–23674. doi:10.1021/jp502119y.
- [13] Q.-S. Du, P.-D. Tang, H.-L. Huang, F.-L. Du, K. Huang, N.-Z. Xie, S.-Y. Long, Y.-M. Li, J.-S. Qiu, R.-B. Huang, A new type of two-dimensional carbon crystal prepared from 1,3,5-trihydroxybenzene, Scientific Reports 7 (2017) 40796. doi:10.1038/srep40796.
  URL https://doi.org/10.1038/srep40796
- [14] C. E. Junkermeier, J. P. Luben, R. Paupitz, N-carbophenes: two-dimensional covalent organic frameworks derived from linear n-phenylenes, MATERIALS RESEARCH EXPRESS 6 (11). doi:10.1088/2053-1591/ab4513.
- [15] C. E. Junkermeier, G. Psofogiannakis, R. Paupitz, Covalent adsorption of functional groups on n-carbophenes, Materials Research Expressdoi:10.1088/2053-1591/ac4c19.
  URL https://doi.org/10.1088/2053-1591/ac4c19
- [16] M. Elstner, D. Porezag, G. Jungnickel, J. Elsner, M. Haugk, T. Frauenheim, S. Suhai, G. Seifert, Self-consistent-charge density-functional tight-binding method for simulations of complex materials properties, Physical Review B 58 (11) (1998) 7260–7268. doi:10.1103/PhysRevB.58.7260. URL http://link.aps.org/doi/10.1103/PhysRevB.58.7260
- [17] B. Aradi, B. Hourahine, T. Frauenheim, DFTB+, a sparse matrix-based implementation of the DFTB method, The Journal of Physical Chemistry A 111 (26) (2007) 5678–5684, pMID: 17567110. arXiv:https://doi.org/10.1021/jp070186p, doi:10.1021/jp070186p. URL https://doi.org/10.1021/jp070186p
- [18] H. Manzano, A. N. Enyashin, J. S. Dolado, A. Ayuela, J. Frenzel, G. Seifert, Do cement nanotubes exist?, Advanced Materials 24 (24) (2012) 3239–3245. doi:10.1002/adma.201103704. URL http://dx.doi.org/10.1002/adma.201103704
- [19] B. Hourahine, B. Aradi, V. Blum, F. Bonafe, C. Buccheri, A.and Camacho, C. Cevallos, M. Y. Deshaye, T. Dumitrica, A. Dominguez, S. Ehlert, M. Elstner, T. van der Heide, J. Hermann, S. Irle, J. J. Kranz, C. Koehler, T. Kowalczyk, T. Kubar, I. S. Lee, V. Lutsker, R. J. Maurer, S. K. Min, I. Mitchell, C. Negre, T. A. Niehaus, A. M. N. Niklasson, A. J. Page, A. Pecchia, G. Penazzi, M. P. Persson, J. Rezac, C. G. Sanchez, M. Sternberg, M. Stoehr, F. Stuckenberg, A. Tkatchenko, V. W. z. Yu, T. Frauenheim, Dftb plus, a software package for efficient approximate density functional theory based atomistic simulations, JOURNAL OF CHEMICAL PHYSICS 152 (12). doi:10.1063/1.5143190.
- [20] J. Frenzel, A. Oliveira, N. Jardillier, T. Heine, G. Seifert, Semi-relativistic, self-consistent charge slater-koster tables for density-functional based tight-binding (DFTB) for materials science simulations, Zeolites 2 (3) (2004) 7. doi:10.3762/bjnano.1.8.
- [21] B. Lukose, A. Kuc, J. Frenzel, T. Heine, On the reticular construction concept of covalent organic frameworks, Beilstein journal of nanotechnology 1 (2010) 60.
- [22] S. A. Hernandez, A. F. Fonseca, Anisotropic elastic modulus, high poisson's ratio and negative thermal expansion of graphynes and graphdiynes, Diamond and Related Materials 77 (2017) 57–64. doi:https://doi.org/10.1016/j.diamond.2017.06.002.
- URL https://www.sciencedirect.com/science/article/pii/S092596351 Setyawan, S. Curtarolo, High-throughput electronic Challenges and tools, Comband structure calculations: putational Materials Science 49 (2) (2010)299-312. doi:https://doi.org/10.1016/j.commatsci.2010.05.010.
- URL https://www.sciencedirect.com/science/article/pii/S092702561
  [24] F. Memarian, A. Fereidoon, M. D. Ganji, Graphene young's modulus: Molecular mechanics and dft treatments, SUPER-LATTICES AND MICROSTRUCTURES 85 (2015) 348-356.

- doi:10.1016/j.spmi.2015.06.001.
- [25] C. Lee, X. Wei, J. W. Kysar, J. Hone, Measurement of the elastic properties and intrinsic strength of monographene, Science 321 (5887) (2008)385-388. arXiv:https://science.sciencemag.org/content/321/5887/385.full.pdf, doi:10.1126/science.1157996.
  - URL https://science.sciencemag.org/content/321/5887/385
- [26] P. L. de Andres, F. Guinea, M. I. Katsnelson, Density functional theory analysis of flexural modes, elastic constants, and corrugations in strained graphene, PHYSICAL REVIEW B 86 (24). doi:10.1103/PhysRevB.86.245409.
- [27] G. Kalosakas, N. N. Lathiotakis, C. Galiotis, K. Papagelis, In-plane force fields and elastic properties of graphene, JOURNAL OF APPLIED PHYSICS 113 (13). doi:10.1063/1.4798384.
- [28] I. Lebedeva, V, A. S. Minkin, A. M. Popov, A. A. Knizhnik, Elastic constants of graphene: Comparison of empirical potentials and dft calculations, PHYSICA E-LOW-DIMENSIONAL SYSTEMS & NANOS-TRUCTURES 108 (2019) 326-338. doi:10.1016/j.physe.2018.11.025.
- [29] L. J. Gibson, M. F. Ashby, Cellular Solids: Structure and Properties, 2nd Edition, Cambridge Solid State Science Series, Cambridge University Press, 1997. doi:10.1017/CBO9781139878326.
- [30] C. Carpenter, A. M. Christmann, L. Hu1, I. Fampiou, A. R. Muniz, A. Ramasubramaniam, D. Maroudas, Elastic properties of graphene nanomeshes, Appl. Phys. Lett. 104. doi:10.1063/1.4871304.
- [31] T. WOIGNIER, J. PHALIPPOU, SCALING LAW VARIATION OF THE MECHANICAL PROPERTIES OF SILICA AEROGELS, Le Journal de Physique Colloques 24 (C4) (1989) C4-179-C4-184. doi:10.1051/jphyscol:1989429.
  - URL https://doi.org/10.1051/jphyscol:1989429
- [32] H. Fan, C. Hartshorn, T. Buchheit, D. Tallant, R. Assink, R. Simpson, D. J. Kisse, D. J. Lacks, S. Torquato, C. J. Brinker, Modulusdensity scaling behaviour and framework architecture of nanoporous self-assembled silicas, NATURE MATERIALS 6 (6) (2007) 418-423. doi:10.1038/nmat1913.
- [33] S. J. Stuart, A. B. Tutein, J. A. Harrison, A reactive potential for hydrocarbons with intermolecular interactions, The Journal of Chemical Physics 112 (14) (2000) 6472-6486. doi:10.1063/1.481208. URL https://doi.org/10.1063/1.481208
- [34] C. E. Junkermeier, Greenwood: A library for creating molecular models and processing molecular dynamics simulations (2018). URL https://github.com/cjunkermeier/greenwood